18TH WORLD CONFERENCE ON EARTHQUAKE ENGINEERING
WCEE2024
MILAN

MILAN, ITALY
30TH JUNE - 5TH JULY 2024

www.wcee2024.it

SEISMIC PERFORMANCE ASSESSMENT OF UNANCHORED MEDICAL EQUIPMENT USING THE CAMERA PROJECTION TECHNIQUE

J. Guamán-Cabrera[1], J.C. de la Llera[2] & D. Mery[3]

[1] Pontificia Universidad Catolica de Chile, Department of Structural & Geotechnical Engineering, Santiago, Chile, jwguaman@uc.cl

[2] Pontificia Universidad Catolica de Chile, Research Center for the Integrated Risk Management of Disasters (CIGIDEN), Santiago, Chile

[3] Pontificia Universidad Catolica de Chile, Department of Computer Science, Santiago, Chile

Abstract: *Lately, several hospitals around the world have lost their medical services due to severe non-structural earthquake-induced damage that occurred within their critical rooms. Currently, there are no code-based performance objectives for unanchored medical equipment subjected to low and strong earthquake motions, and consequently, loss of functionality is expected for building design levels of demand. Aiming to shed some light on this gap, this paper uses the Camera Projection Technique (CPT) to extract the dynamic response of the medical equipment installed at the fourth and fifth levels of the full-scale, five-story RC building tested at the University of California, San Diego (UCSD) in 2012, considering both Fixed to the Base (FB) and Base Isolated (BI) support conditions. In the CPT approach, a mapping process between the 3D space and the 2D images of the camera videos is performed to continuously track the position of the equipment. The camera network was comprised of IP and COAX cameras strategically deployed in the UCSD building. It was found that CPT accurately extracted not only the horizontal displacements and in-plane rotations but also the rocking and toppling responses of the medical equipment as long as neither significant impacts nor inertial mass changes occurred during the shakings. Finally, more experimental campaigns of unanchored medical equipment, including electronic functionality tests, would be required to adequately characterize its damage*.

1. Introduction

Hospital buildings are conceptualized as centers of immediate response during disaster scenarios as they receive and shelter injured people until their full recovery. However, it has become common to learn that hospitals lost their medical provision capacity during earthquake events due to the significant non-structural damage suffered within their critical rooms. For instance, Ayres et al. (1973); Mitrani et al. (2012); Kagermanov et al. (2017); Santarsiero et al. (2019); and Dilsiz et al. (2023) are just a few examples of post-earthquake non-structural damage reports that describe the impact on loss of functionality.

The lack of a comprehensive gathering of post-earthquake damage information is one of the main reasons that has prevented scientists and researchers from accurately characterizing non-structural damage. Since most of the debris and rubble is frequently cleaned up within hours after the disaster, there is little non-structural damage information that can be adequately retrieved by the reconnaissance teams. Because of this, it has been necessary to explore other means to characterize the behavior of non-structural components during earthquake motions.

During the last decades, some researchers have tried to reproduce the dynamic behavior of certain medical equipment resorting to simple rigid block analogies such as Housner (1963); Yim et al. (1980); Shenton and Jones (1991), among others. On the other hand, some investigators have used shake-table experiments to test laboratory equipment like Chaudhuri and Hutchinson (2005); hospital equipment in Konstantinidis and Makris (2008); medical cabinets in Cosenza et al. (2015); Di Sarno et al. (2019); and Petrone et al. (2017); ultrasounds and casters in Nikfar and Konstantinidis (2017a); and automatic hematology and coagulation analyzers in Yu et al. (2023).

Recently, full-scale, mid-rise steel and concrete buildings containing real hospital contents have been tested to assess the non-structural behavior and interaction with the structural response. For instance, in the experiments executed by the E-Defense in collaboration with the University of Nevada, Reno, in 2014, a five-story steel moment frame building with two different isolation systems and fixed-to-the-base (FB) support condition was tested considering the fourth level as a hospital room and the fifth level as an office room. In this study, Guzman Pujols and Ryan (2016) developed qualitative fragility functions that estimate the level of disruption achieved by hospital and office contents as a whole. Similarly, a four-story reinforced concrete (RC) building with two different isolation systems and FB support conditions was tested at the E-Defense facility in Japan between 2008-2009. Here, an Operation Room (OR) located on the third level was tested containing an operation table, an electric laser machine, a cardioverted defibrillator, a heart-lung machine, and a ceiling pendant. Shi et al. (2014) studied the damage and disorder of this room presenting a quantitative assessment of the medical devices including friction coefficients, maximum displacements, impacts, and trajectory orbits.

In 2012, the University of California in San Diego tested a full-scale, five-story RC building considering two different support conditions, namely, FB and Base-Isolated (BI). An Intensive Care Unit (ICU) was replicated at the fourth level, while an OR was simulated at the fifth level. The building was subjected to twelve different earthquake motions of increasing intensity to gradually produce damage in the structure and non-structural elements from linear behavior to above design levels of demand as explained in Chen et al. (2013a). Hereafter this building will be referred to as the UCSD building. This study presents quantitative and qualitative structural damage descriptions associated with each level of motion. Additionally, qualitative non-structural damage descriptions for drywall partitions, systems, ceilings, and medical equipment are provided. This information can be accessed at the DesignSafe-CI platform (NEES-2009-0722 Project) in Hutchinson et al. (2012).

On the other hand, current codes, and standards such as the ASCE/SEI 7-22 (2002); NIST (2018); FEMA E-14 (2012); and CEN-Eurocode 8 (2004) have not provided specific performance objectives for medical equipment, mainly due to the limited information available of the non-structural performance, and to the lack of consensus among experts. Consequently, quantitative requirements have not been established yet for medical content. Aiming to reduce this gap, recently, Guamán-Cabrera et al. (2023) were able to reproduce the horizontal rolling displacements and toppling responses of the medical equipment deployed in the UCSD building test. This study used the Camera Projection Technique (CPT) to extract the equipment's experimental displacement and toppling responses from different floor input motions. Moreover, two nonlinear models, namely, rolling and toppling, were developed to reproduce the experimental responses obtained through CPT. This investigation found that both models were able to accurately reproduce the equipment displacement, and toppling cases as long as no impacts or considerable loss of inertial mass occurs.

The present paper proposes the CPT as a visual-based valid approach to assess the seismic performance of some pieces of medical equipment located at the UCSD building. Further information about the rolling and toppling nonlinear numerical models used to reproduce the experimental responses can be found in Guamán-Cabrera et al. (2023). In agreement with this latter study, the present paper is based on the technical BNCS reports 1 through 4 presented by Chen et al. (2013a, 2013b) and Pantoli et al. (2013a, 2013b), as well as the publicly available UCSD structural and non-structural information at DesignSafe-CI platform.

2. Medical equipment description

Detailed information about the UCSD building, materiality, construction process, and test protocols can be found in the BNCS reports 1 through 4. Similarly, the structural and nonstructural responses and videos can be accessed on the DesignSafe-CI platform. As it was mentioned, the fourth building level was intended to represent an ICU, whereas the fifth floor was simulated as an OR. Figure 1 depicts the location of the medical equipment considered in this paper and installed at the fourth and fifth levels, respectively.

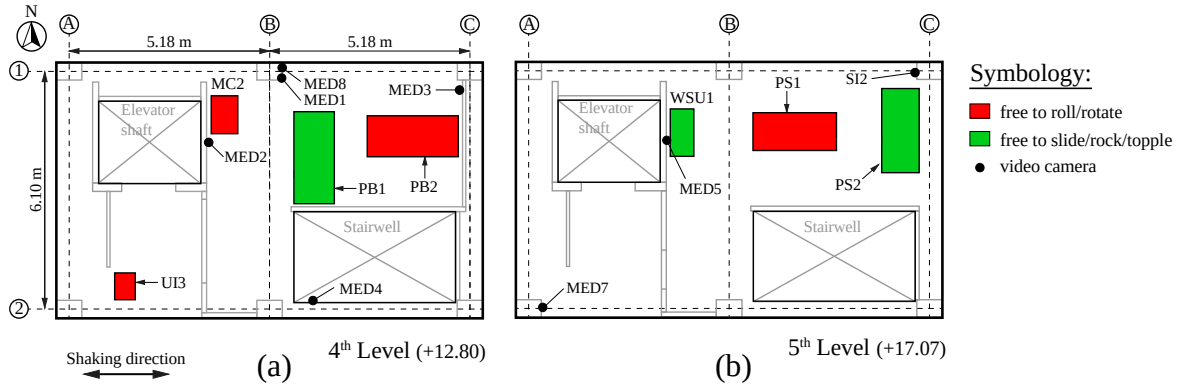

Figure 1. Medical equipment deployed on the (a) fourth and (b) fifth levels showing the ability to roll, slide, rock, or topple. Locations of video cameras to record non-structural motion are indicated as black solid dots.

It is important to mention that Figure 1 shows only the equipment having the rolling, sliding, rocking, and toppling behavior. Medical equipment attached to partition walls, anchored to the floor concrete slab, or hanging down from the concrete slab is out of the scope of this paper. Finally, Figure 1 indicates the in-plane location of the video cameras used to record the equipment motion. It should be mentioned that only two pieces of this equipment, namely, PS1 and PS2, will be analyzed in the present paper.

2.1. Medical equipment at the fourth level

The equipment, shown in Figure 1a, and located at the fourth level was comprised of (a) locked patient bed PB1; (b) unlocked patient bed PB2; (c) unlocked mobile cart MC2; and (d) unlocked ultrasound imager UI3. The first equipment was free to rock and topple, whereas the rest was free to roll and rotate.

2.2. Medical equipment at the fifth level

As shown in Figure 1b, the equipment located at the fifth level was comprised of (a) an unlocked stretcher PS1 free to roll and rotate; (b) a locked stretcher PS2 free to rock and topple; and (c) a free-standing wire shelving unit WSU1 free to slide and topple.

3. Input motions

Table 1 presents the earthquake motions used in the UCSD test for BI and FB support conditions. Information about the natural frequency of the above-described equipment can be found in Guamán-Cabrera et al. (2023).

Table 1. List of earthquake motions used in the UCSD building test. (Chen et al, 2012)

Name	Earthquake Event-Site (Scaling %)	PIA[1] (g)	PIV[1] (cm/s)	PID[1] (cm)
BI-1: CNP100	1994 Northridge-Canoga Park (100)	0.21	23.37	8.42
BI-2: LAC100	1994 Northridge-LA City Terrace (100)	0.25	24.48	8.95
BI-3: SP100	2010 Maule (Chile)-San Pedro (100)	0.52	34.87	8.27
BI-4: ICA50	2007 Pisco (Peru)-Ica (50)	0.17	22.32	4.76
BI-5: ICA100	2007 Pisco (Peru)-Ica (100)	0.32	42.59	9.46
BI-6: ICA140	2007 Pisco (Peru)-Ica (140)	0.50	62.59	12.92
FB-1: CNP100	1994 Northridge-Canoga Park (100)	0.21	23.50	8.78
FB-2: LAC100	1994 Northridge-LA City Terrace (100)	0.18	23.05	9.31
FB-3: ICA50	2007 Pisco (Peru)-Ica (50)	0.21	26.22	5.83
FB-4: ICA100	2007 Pisco (Peru)-Ica (100)	0.26	28.49	7.32
FB-5: DEN67	2002 Denali-TAPS Pump St. #9 (67)	0.64	63.74	20.06
FB-6: DEN100	2002 Denali-TAPS Pump St. #9 (100)	0.80	83.57	33.62

[1] Achieved Peak Input Acceleration (PIA), Velocity (PIV), and Displacement (PID) on the shake table.

4. Video cameras

The UCSD building was equipped with a large video camera network to record the motion during the seismic tests inside and outside the building. Particularly, the camera network installed inside the building was intended to solely provide insight into the movement, interaction, and disorder of the non-structural elements, systems, and contents (*NSC*), and not to intentionally perform a vision-based motion tracking of any medical equipment. The movement of medical equipment was recorded by Internet Protocol (IP) and Coaxial cable (COAX) cameras installed on each floor. There were 56 IP cameras and 16 COAX cameras distributed within the building. The IP cameras, manufactured by Vivotek, had a model: IP8332-Network Bullet Camera, whereas the COAX cameras, manufactured by Sony, were either VC-CA-IR120 Infrared Camera or X-Treme Military Grade Night Bullet Camera. The IP cameras were equipped with an IMP sensor to allow a 1280x800 resolution at 30 fps (frames per second) as described in Chen et al. (2013a). Figures 2a and 2b show the location of some IP cameras deployed at the fourth and fifth levels, respectively.

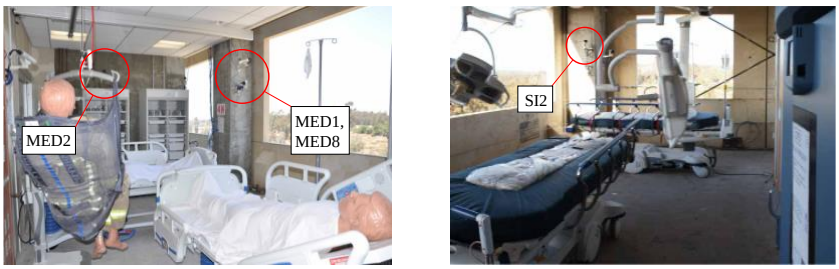

(a) (b)

Figure 2. IP cameras located at the (a) fourth and (b) fifth levels to record medical equipment movement. Source: Photos courtesy of Professor Tara Hutchinson.

5. Camera projection technique (CPT)

Ideally, a vision-based motion tracking procedure such as the one implemented by Nikfar and Konstantinidis (2017b) should be used to estimate the equipment response. Nevertheless, and due to the fact that vision-based motion tracking was not conceived in the UCSD test, it was necessary to resource other techniques to assess the performance of the mobile medical equipment. Based on this and taking advantage of the camera network installed, the Camera Projection Technique (CPT) was adopted as a valid approach to extract the medical equipment dynamic responses.

5.1. Camera model

According to Hartley and Zisserman (2004), a camera is defined as a mapping between the 3D space and a 2D image. The camera used in this paper is the *central projection*, and the camera model adopted is the pinhole camera model, which is the most specialized and simplest. In this model, the central projection of a point in 3D space with Euclidean coordinates $(X, Y, Z)^T$ is mapped to a 2D point $(u, v)^T$ on the image plane, as shown in Figure 3.

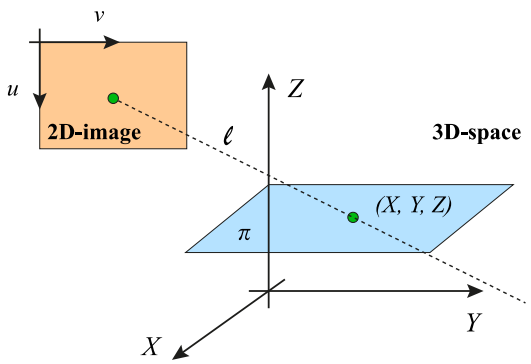

Figure 3. Pinhole camera projection model. Ref. Guamán-Cabrera et al. (2023).

5.2. Camera projection matrix P

The projection, shown in Figure 3, can be expressed through Euclidean coordinates as explained in Hartley and Zisserman (2004); and Guamán-Cabrera et al. (2023):

$$\lambda \begin{bmatrix} u \\ v \\ 1 \end{bmatrix} = \begin{bmatrix} p_{11} & p_{12} & p_{13} & p_{14} \\ p_{21} & p_{22} & p_{23} & p_{24} \\ p_{31} & p_{32} & p_{33} & p_{34} \end{bmatrix} \begin{bmatrix} X \\ Y \\ Z \\ 1 \end{bmatrix}, \quad (1)$$

where λ is a scale factor and p_{ij} are the elements of the 3×4 projection matrix **P**. This projection matrix can be obtained by using a calibration approach as described in Hartley and Zisserman (2004) with known pair points $(X_k, Y_k, Z_k) \leftrightarrow (u_k, v_k)$, for $k = 1 \cdots n$, and $n \geq 8$. It has been found that eight or more calibration points notably improve the tracking process of the moving object whereas a smaller number of points might cause unsuccessful tracking. Generally, the 3D points (X_k, Y_k, Z_k) are given in millimeters and the 2D points (u_k, v_k) in pixels. The 3D coordinates correspond to real physical points with Euclidean coordinates that can be readily obtained and verified on-site, and they are referred to as *fixed points* in this paper. On the other hand, the 2D coordinates of the image are extracted from the initial video frame. A script developed in Python was used to load the video and to locate both, 3D and 2D coordinates with different colors (see Figures 4a and 5a). By proceeding this way, it is easier to adjust the 2D coordinates, if needed, to reduce the difference between both types of coordinates during the calibration process.

The calibration is an optimization process that estimates the matrix **P** by minimizing the following objective function as indicated in Hartley and Zisserman (2004) and Guamán-Cabrera et al. (2023):

$$J(\mathbf{P}) = \frac{1}{n} \sum_{k=1}^{n} \sqrt{(u_k - \hat{u}_k)^2 + (v_k - \hat{v}_k)^2} \rightarrow \min \quad (2)$$

where $(\hat{u}_k, \hat{v}_k)$ are the coordinates of the *k-th* projected point using Equation 1 and the coordinates of the fixed points (X_k, Y_k, Z_k). The exact location of the objective 3D point may be known by considering the plane π in the 3D space, on which the 3D point lies. This plane can be defined as expressed in Hartley and Zisserman (2004) and Guamán-Cabrera et al. (2023):

$$\pi: aX + bY + cZ + d = 0 \quad (3)$$

A system of three linear equations with three unknowns (X, Y, Z) can be obtained after manipulating Equations 1 and 3, knowing the parameters of the plane (a, b, c, d) and the elements p_{ij} of the estimated projection matrix **P**. The solution to this system results:

$$\begin{bmatrix} X \\ Y \\ Z \end{bmatrix} = -\begin{bmatrix} p_{11} - p_{31}u & p_{12} - p_{32}u & p_{13} - p_{33}u \\ p_{21} - p_{31}v & p_{22} - p_{32}v & p_{23} - p_{33}v \\ a & b & c \end{bmatrix}^{-1} \begin{bmatrix} p_{14} - p_{34}u \\ p_{24} - p_{34}v \\ d \end{bmatrix} \quad (4)$$

5.3. Tracking of the moving point

The 3D trajectory of any moving point within a 3D scene can be estimated by manually selecting a 2D point (u_0, v_0) on the first frame of the sequence (for $t = 0$) that lies on a known plane π in 3D space. This point is then tracked automatically across the next frames ($t > 0$) of the video. The tracking of the moving point in the video sequence can be achieved by following the next steps as indicated in Szeliski, (2022):

1) For $t = 0$ define a small window $\boldsymbol{W}_t$ centered in (u_t, v_t) and of size $m \times m$ pixels (e.g. $m = 20$).

2) In the next frame, search for a window $\boldsymbol{W}_{t+1}$ of size $m \times m$ pixels in the neighborhood of (u_t, v_t) with the closest similarity to the window $\boldsymbol{W}_t$, i.e.

$$\left|\left|\boldsymbol{W}_t - \boldsymbol{W}_{t+1}\right|\right| \rightarrow \min \quad (5)$$

3) Update (u_{t+1}, v_{t+1}) with the location of the center of $\boldsymbol{W}_{t+1}$ and repeat the process starting from step 2 and using $t \leftarrow t + 1$ until the end of the sequence of the video frames.

6. Vision-based tracking using CPT

The vision-based tracking procedure using CPT can be summarized as described in Guamán-Cabrera et al. (2023): 1) Load the video and extract its frames, number of frames, the frame rate of the camera in fps (frames per second), width and height of the frames in pixels; and duration of the video in seconds. 2) Arbitrarily define at least eight coordinates (in mm) of the 3D points (fixed points) that will be located on the first frame of the 2D image. Ideally, none of the fixed points shall be hidden by any moving object during the whole frame sequence of the video. 3) Extract the corresponding 2D coordinates (in pixels) of the 3D points to pair them. Both, 3D and 2D points are referred to as *Calibration Points.* 4) Adjust the 2D coordinates if necessary to match the 2D points with the 3D points on the image. 5) Obtain the projection matrix **P** using Equations 1 and 2. 6) Define 3D and 2D coordinates of the moving point (target) to be tracked. 7) Once the location of the moving point has been defined, the plane $\boldsymbol{\pi}$ can be obtained from Equation 3. 8) After estimating the matrix **P** and defining the plane $\boldsymbol{\pi}$, the 3D coordinates of any point lying on the plane $\boldsymbol{\pi}$ can be extracted using Equation 4. 9) Track the selected moving point using the procedure indicated in Section 5.3 and Equation 5. 10) Verify that the moving point is being continuously tracked in all frames of the sequence. An algorithm developed in Python was used to implement this procedure.

7. Results

7.1. Rolling equipment performance

As an example of the CPT, the rolling displacement of the unlocked stretcher PS1 located at the fifth level of the UCSD building and subjected to the BI-1: CNP100 motion is presented in Figure 4. Figure 4a displays fourteen 3D fixed points (red circular dots) overlapped with the 2D points (blue circular dots) for calibration purposes. Note that these calibration points are evenly distributed within the scene. Also, two moving points, namely, M1 and M2 (yellow circular dots) were chosen on the stretcher's side rail. These latter points were selected after several tracking trials performed on different positions on the stretcher. M1 and M2 resulted to be the brightest points that could be fully tracked during all the sequence of frames (*N*=1,000). It should be mentioned that the proximity between the 3D and 2D points must be checked before each tracking trial to update the projection matrix **P** accordingly.

After selecting points M1 and M2, the plane π in 3D space is defined by the height of these points. Figure 4b shows the tracking of M1 in the first two video frames. Figure 4c shows the full tracking of points M1 and M2 for the whole frame sequence (*N*=1,000). Figure 4d displays the horizontal rolling displacement trails of M1 and M2 for the sequence considered. Figure 4e displays the X and Y displacements of M1 and M2. The green connecting lines help to visualize the in-plane rotation of these moving points. Also note that at the end of the motion, this stretcher experienced a repeatedly forward and backward movement. Finally, Figure 4f shows a graphical comparison of X and Y rolling displacements versus the number of frames. It can be observed that the stretcher displacements in the X direction (longitudinal) were considerably larger than those observed in the Y direction (transversal). This expected outcome is due to the input motion direction (longitudinal). A similar analysis was performed for the unlocked patient bed PB2, mobile metal cart MC2, and ultrasound imager UI3 located at the 4th building level. These assessments can be found in Guamán-Cabrera et al. (2023). The rolling displacements were verified against the initial and final positions of each equipment during the tests.

7.2. Rocking equipment performance

Following a similar procedure, Figure 5 shows the performance of the locked stretcher PS2 located at the fifth level and subjected to the FB4: ICA100 motion. Due to its orientation (90° with respect to the input motion) and support condition (brakes fully engaged), this stretcher experienced rocking motion behavior and eventually toppled after the rocking angle exceeded the critical rotation angle. As before, Figure 5a displays ten 3D fixed points (red circular dots) overlapped with the 2D points (blue circular dots) for the calibration analysis. Similarly, two points, M1 and M2 (yellow circular dots) located on the stretcher's side rail were selected as tracking points. Figure 5b shows the tracking of point M1 in the first two frames. Figure 5c confirms that both points, M1 and M2, were continuously tracked during the frame sequence (*N*=1,000). Figure 5d displays the displacement trails of M1 and M2 for the sequence considered. The green connecting lines, shown in Figure 5e, help to visualize the rocking-toppling phenomenon. Finally, Figure 5f shows the 3D displacements of points M1 and M2. A similar analysis was carried out for the locked patient bed PB1, and wire shelving unit WSU1 located at the 4th and 5th levels, respectively, and presented in Guamán-Cabrera et al. (2023).

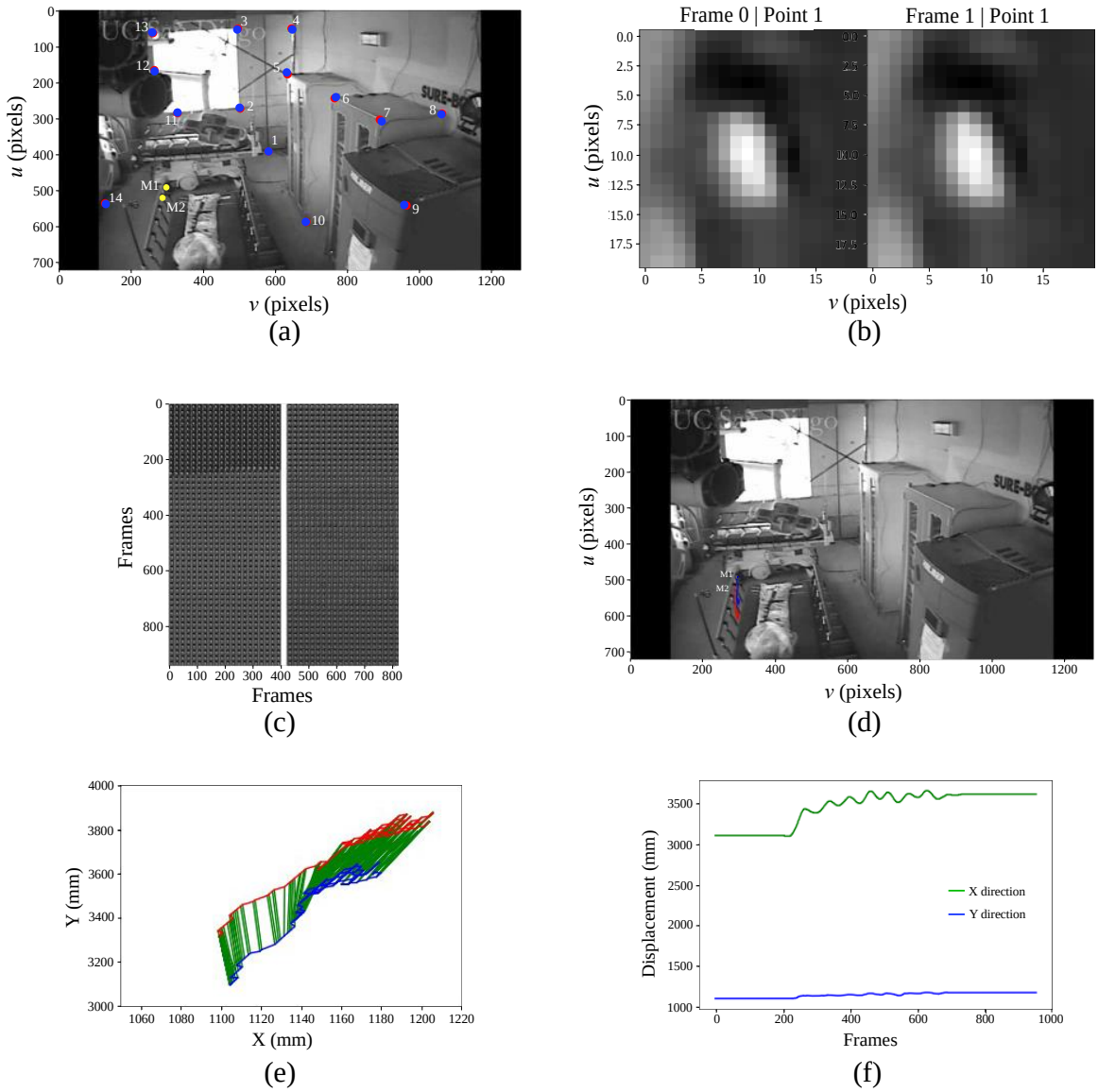

Figure 4. Camera Projection Technique (CPT) applied to unlocked patient stretcher PS1 during the BI-1: CNP100 motion: (a) 2D fixed and moving points overlapped in frame 0; (b) bright moving point M1 being tracked from frame 0 to frame 1; (c) video frames showing successful tracking of points M1 and M2; (d) horizontal rolling displacement trails of points M1 and M2; (e) X and Y rolling displacement trajectories; (f) X and Y displacements versus number of frames. (Ref. Guamán-Cabrera et al., 2023).

8. Conclusions

The dynamic behavior and seismic performance of the unanchored medical equipment deployed at the full-scale, five-story RC building tested at the University of California San Diego (UCSD) in 2012 for both, Fixed-to-the Base (FB) and Base Isolated (BI) support conditions have been assessed. As per this paper, the following conclusions can be presented:

- The Camera Projection Technique (CPT) has been proven to be a valid approach to estimating the rolling and rocking behavior of unanchored medical equipment.
- It was found that CPT was capable of extracting not only the horizontal rolling displacements and in-plane rotations, but also the rocking behavior and toppling occurrences as long as neither severe impacts nor significant changes in the inertial mass occurred.

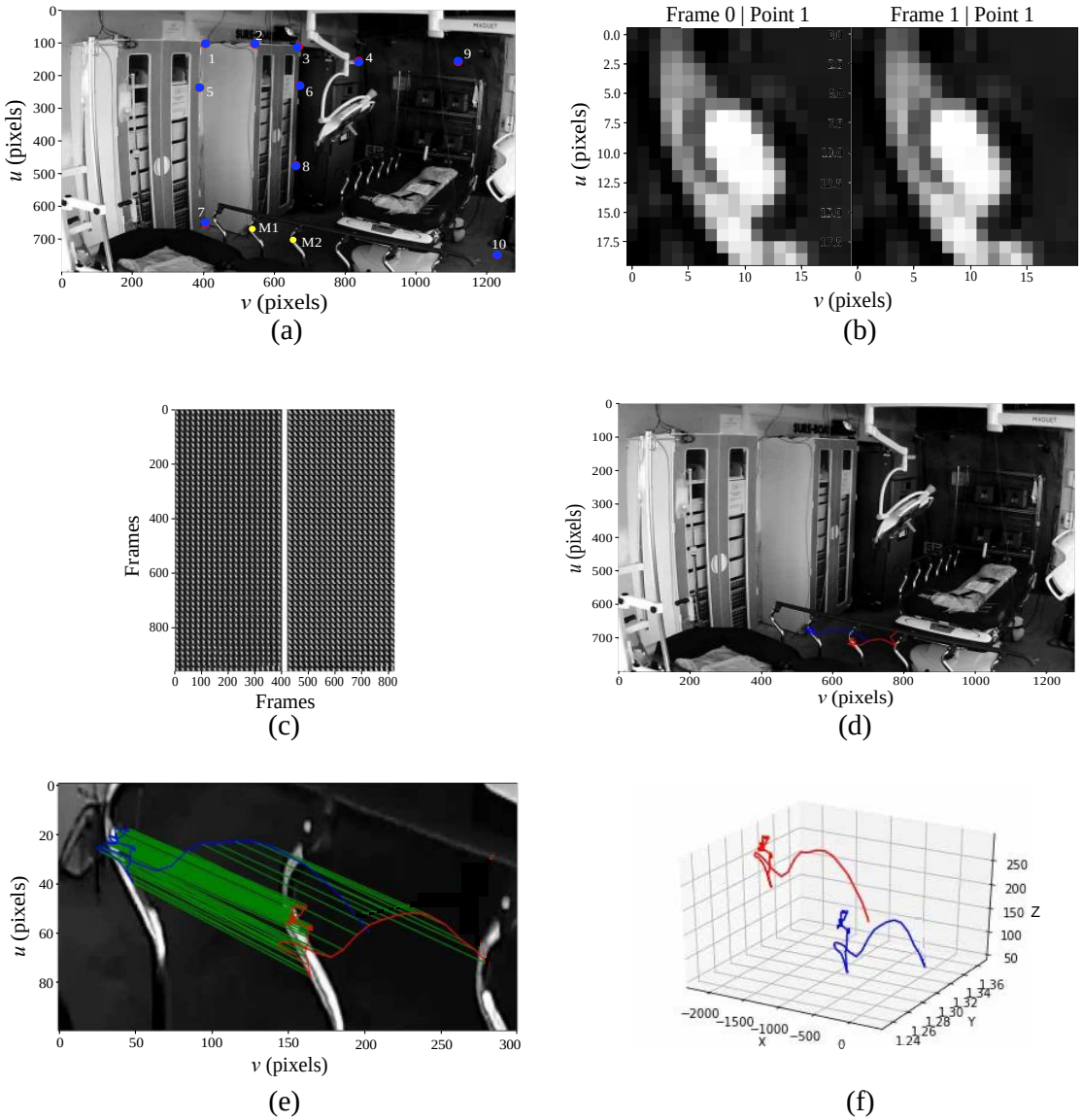

Figure 5. Camera Projection Technique (CPT) applied to locked patient stretcher PS2 during the FB-4: ICA100 motion: (a) 2D fixed and moving points overlapped in frame 0; (b) bright moving point M1 being tracked from frame 0 to frame 1; (c) video frames showing successful tracking of points M1 and M2; (d) rocking motion trails of points M1 and M2; (e) 3D displacement trajectories; (f) X, Y, and Z displacements. (Ref. Guamán-Cabrera et al., 2023).

9. References

ASCE, 2022. Minimum Design Loads and Associated Criteria for Buildings and Other Structures-American Society of Civil Engineers (2022), American Society of Civil Engineers, Reston, VA.

Ayres J., Sun T., and Brown, F. (1973). “Non-structural Damage to Buildings” In the Great Alaska Earthquake of 1964, *National Academy of Sciences, Washington D.C.*

CEN (2004). Eurocode 8: Design provisions for earthquake-resistant structures. Comité Européen de Normalisation, Brussels, Belgium.

Chaudhuri S., and Hutchinson T. (2005). Performance Characterization of Bench-and Shelf-Mounted Equipment, Pacific Earthquake Engineering Center, Berkley, CA.

Chen M., Pantoli E., Wang X., Astroza R., Ebrahimian H., Mintz S., Hutchinson T., Conte J., and Restrepo J., Meacham B., Kim J., and Park H., (2013a). BNCS Report #1: Full-scale Structural and Nonstructural Building System Performance During Earthquakes and Post-Earthquake Fire – Specimen Design,

Construction, and Test Protocol, Department of Structural Engineering, University of California, San Diego, CA.

Chen M., Pantoli E., Wang X., Mintz S., Hutchinson T., and Restrepo J. (2013b). BNCS Report #4: Full-scale Structural and Nonstructural Building System Performance During Earthquakes and Post-Earthquake Fire – Construction Details and Technical Specifications of Specific Subsystems. Department of Structural Engineering, University of California, San Diego, CA.

Cosenza E., di Sarno L., Maddaloni G., Magliulo G., Petrone C., and Prota A. (2015). Shake table tests for the seismic fragility evaluation of hospital rooms, Earthquake Engineering & Structural Dynamics, 44(1): 23–40.

Di Sarno L., Magliulo G., D'Angela D., and Cosenza E. (2019). Experimental assessment of the seismic performance of hospital cabinets using shake table testing. Earthquake Engineering & Structural Dynamics, 48(1): 103-123.

Dilsiz A., Günay S., and Mosalam K. (2023). Joint preliminary virtual reconnaissance report (PVRR): 2023 Türkiye Earthquake Sequence. *Building Resilience through Reconnaissance*.

FEMA E-14 (2012). Reducing the Risks of Nonstructural Earthquake Damage, ATC-58, Applied Technology Council, Washington, D.C.

Guamán-Cabrera J., De la Llera J.C., and Mery D. (2023). Seismic performance assessment of medical equipment using experimentally validated rolling and toppling nonlinear models. *Earthquake Spectra*, 39(3):1810-1836.

Guzman Pujols J. C., and Ryan K. L. (2016). Development of generalized fragility functions for seismically induced content disruption. *Earthquake Spectra*, 32(3): 1303–1324.

Hartley R., and Zisserman A. (2004). Multiple view geometry in computer vision. 2nd edition. Cambridge University Press.

Housner G. W. (1963). The behavior of inverted pendulum structures during earthquakes. *Bulletin of the Seismological Society of America*, 53(2): 403–417.

Hutchinson, T., Restrepo, J., Conte, J., Pantoli, E., Chen, M., Wang, X., Astroza, R., and Ebrahimian, H., (2012). Shake Table Testing of a Five-Story Building Outfitted with NCSs (BNCS project). DesignSafe-CI, San Diego, CA.

Kagermanov A., Ceresa P., Morales E., Poveda J., and O'Connor J. (2017). Seismic performance of RC buildings during the MW7.8 Muisne (Ecuador) earthquake on April 2016: field observations and case study. *Bulletin of Earthquake Engineering*, 15(12): 5167–5189.

Konstantinidis D., and Makris N. (2008). Experimental and analytical studies on the response of freestanding laboratory equipment to earthquake shaking. Earthquake Engineering & Structural Dynamics, 38(6): 827–848.

Mitrani-Reiser J., Mahoney M., Holmes W.T., De la Llera J.C., Bissell R., and Kirsch T. (2012). A Functional Loss Assessment of a Hospital System in the Bio-Bio Province. *Earthquake Spectra*, 28(S1): 473–502.

Nikfar F., and Konstantinidis D., (2017a). Shake table investigation on the seismic performance of hospital equipment supported on wheels/casters. Earthquake Engineering & Structural Dynamics, 46(2): 243–266.

NIST (2018). Recommendations for Improved Seismic Performance of Nonstructural Components. National Institute of Standards and Technology, Gaithersburg, MD, NIST GCR 18-917-43.

Pantoli E., Chen M., Wang X., Astroza R., Ebrahimian H., Mintz S., Hutchinson T., Conte J., and Restrepo J., (2013a). BNCS Report #2: Full-scale Structural and Nonstructural Building System Performance During Earthquakes and Post-Earthquake Fire – Test Results. Department of Structural Engineering, University of California, San Diego, CA.

Pantoli E., Chen M., Hutchinson T., and Restrepo J., (2013b). BNCS Report #3: Full-scale Structural and Nonstructural Building System Performance During Earthquakes and Post-Earthquake Fire – Camera and Analog Sensor Details. Department of Structural Engineering, University of California, San Diego, CA.

Petrone C., di Sarno L., Magliulo G., and Cosenza E. (2017). Numerical modelling and fragility assessment of typical freestanding building contents. *Bulletin of Earthquake Engineering*, 15: 1609–1633.

Santarsiero G., Di Sarno L., Giovinazzi S., Masi A., Cosenza E., and Biondo S. (2019). Performance of the healthcare facilities during the 2016-2017 Central Italy seismic sequence. *Bulletin Earthquake Eng*ineering, 17: 5701-5727.

Shenton III, H. W., and Jones N. P. (1991). Base excitation of rigid bodies. I: Formulation. *Journal of Engineering Mechanics*, 117(10): 2286–2306.

Shi Y., Kurata M., and Nakashima M. (2014). Disorder and damage of base-isolated medical facilities when subjected to near-fault and long-period ground motions. *Earthquake Engineering and Structural Dynamics*, 43(11):1683-1701.

Szeliski R. (2022). Computer vision: algorithms and applications. *Springer Nature*.

Yim C.-S., Chopra A. K., and Penzien J. (1980). Rocking response of rigid blocks to earthquakes. *Earthquake Engineering & Structural Dynamics*, 8(6): 565–587.

Yu P., Zhai C., Liu J., and Wang X. (2023). Shake table tests for the seismic performance assessment of desktop medical laboratory equipment considering the effect of adjacent walls and restrainers. Structures, 50: 1922-1933.